Atmos. Chem. Phys. Discuss., 9, 11441–11479, 2009
www.atmos-chem-phys-discuss.net/9/11441/2009/

Atmospheric Chemistry and Physics Discussions

This discussion paper is/has been under review for the journal *Atmospheric Chemistry and Physics (ACP)*. Please refer to the corresponding final paper in *ACP* if available.

Tropospheric ozone from IASI: comparison of different inversion algorithms and validation with ozone sondes in the northern middle latitudes

C. Keim[1,*], M. Eremenko[1], J. Orphal[1], G. Dufour[1], J.-M. Flaud[1], M. Höpfner[2], A. Boynard[3], C. Clerbaux[3], S. Payan[4], P.-F. Coheur[5], D. Hurtmans[5], H. Claude[6], H. Dier[7], B. Johnson[8], H. Kelder[9], R. Kivi[10], T. Koide[11], M. López Bartolomé[12], K. Lambkin[13], D. Moore[14], F. J. Schmidlin[15], and R. Stübi[16]

[1]Laboratoire Interuniversitaire des Systèmes Atmosphériques (LISA), CNRS/Univ. Paris 12 et 7, Créteil, France
[2]Institut für Meteorologie und Klimaforschung, Forschungszentrum Karlsruhe, Germany
[3]UPMC Univ. Paris 06, CNRS UMR8190, LATMOS/IPSL, Paris, France
[4]Laboratoire de Physique Moléculaire pour l'Atmosphére et l'Astrophysique, Université Pierre et Marie Curie-Paris 6, Paris, France

[5] Spectroscopie de l'Atmosphère, Service de Chimie Quantique et de Photophysique, Université Libre de Bruxelles (U.L.B.), Brussels, Belgium
[6] Meteorological Observatory Hohenpeißenberg, DWD, Hohenpeißenberg, Germany
[7] Richard-Aßmann-Observatorium, DWD, Lindenberg, Germany
[8] NOAA/ESRL, Boulder, CO, USA
[9] Department of Applied Physics, Eindhoven University of Technology, Eindhoven, The Netherlands
[10] Finnish Meteorological Institute, Sodankylä, Finland
[11] Ozone Layer Monitoring Office, Japan Meteorological Agency, Tokyo 100-8122, Japan
[12] Agencia Estatal de Meteorología (AEMET), Madrid, Spain
[13] Met Éireann, The Irish Meteorological Service, Valentia Observatory, Cahirciveen, Kerry, Ireland
[14] Met Office, Exeter, UK
[15] NASA Goddard Space Flight Center, Wallops Flight Facility, Wallops Island, USA
[16] Federal Office of Meteorology and Climatology, MeteoSwiss, Aerological Station, Payerne, Switzerland
[*] now at: Astrium GmbH, Germany

Received: 24 February 2009 – Accepted: 11 April 2009 – Published: 8 May 2009

Correspondence to: M. Eremenko (maxim.eremenko@lisa.univ-paris12.fr)

Published by Copernicus Publications on behalf of the European Geosciences Union.

Abstract

This paper presents a first statistical validation of tropospheric ozone products derived from measurements of the satellite instrument IASI. Since end of 2006, IASI (Infrared Atmospheric Sounding Interferometer) aboard the polar orbiter Metop-A measures infrared spectra of the Earth's atmosphere in nadir geometry. This validation covers the northern mid-latitudes and the period from July 2007 to August 2008. The comparison of the ozone products with the vertical ozone concentration profiles from balloon sondes leads to estimates of the systematic and random errors in the IASI ozone products. The intercomparison of the retrieval results from four different sources (including the EUMETSAT ozone products) shows systematic differences due to the used methods and algorithms. On average the tropospheric columns have a small bias of less than 2 Dobson Units (DU) when compared to the sonde measured columns. The comparison of the still pre-operational EUMETSAT columns shows higher mean differences of about 5 DU.

1 Introduction

Ozone is a key species in the photochemistry of the troposphere and is a pollutant with significant impact on health and agriculture (Seinfeld and Pandis, 1998). It is also an important greenhouse gas with strong radiative forcing in the upper troposphere (Fishman et al., 1979). Monitoring of tropospheric ozone is extremely important for the understanding and quantification of air pollution (including the possibility to distinguish between local sources and long-range transport of pollution) and to predict and engineer air quality at the local and regional scales. Ozone concentrations are currently measured at the surface level using national operational networks, furthermore vertical concentration profiles are measured at selected sites using meteorological balloon sondes. In this context, satellite observations in nadir geometry are very interesting because of their high spatial coverage, but such observations are limited in terms of

ACPD

9, 11441–11479, 2009

temporal coverage (typically 1–2 measurements per day for a given location), and they are particularly difficult for tropospheric ozone because the stratospheric ozone layer contains the main part of the ozone total column. Vertical resolution is therefore a crucial issue for satellite measurements of tropospheric ozone.

The first satellite measurements of tropospheric ozone have been obtained from instruments measuring solar reflected and backscattered light using residual techniques (Fishman et al., 2003) but have limitations especially in mid- and high latitudes. More recently, using atmospheric spectra in the ultraviolet-visible from instruments like GOME (Liu et al., 2005), tropospheric ozone columns have been obtained but again with little information in the mid- and high latitudes. It has been demonstrated (Turquety et al., 2002; Coheur et al., 2005) that atmospheric spectra in the thermal infrared can provide accurate measurements of tropospheric ozone, with the additional advantage that measurements are also possible during the night. In particular, the TES (Tropospheric Emission Spectrometer) instrument aboard the EOS-Aura satellite has provided measurements of tropospheric ozone (Worden et al., 2007) with first applications to air quality modelling (Jones et al., 2008) and climate (through an estimate of its radiative forcing) (Worden et al., 2008). More recently, the European IASI (Infrared Atmospheric Sounding Interferometer) instrument aboard the Metop-A satellite (launched in late 2006) has started with operational measurements in summer 2007. In contrast to TES, IASI has very high spatial coverage and is therefore well suited for measurements of tropospheric ozone with an air quality focus. A first study of tropospheric ozone during the heat wave over Europe in summer 2007 has been published very recently (Eremenko et al., 2008), demonstrating the great potential of IASI measurements for air quality applications.

In the present paper, we describe the first general comparison of tropospheric ozone products obtained using different inversion algorithms and methods, but based on exactly the same IASI measurements, and the validation of these products using vertical ozone concentration profiles obtained from balloon sondes. This study is in particular important to identify possible systematic errors or biases in the tropospheric ozone

products.

The paper is organised as follows: first, after a short introduction focusing on the IASI instrument, the different retrieval methods and inversion algorithms are presented. The second part describes the in-situ measurements and the coincidence criteria for the validations. In the third part, the methods and results of the different comparisons are shown and discussed.

2 The IASI instruments on Metop

IASI (Infrared Atmospheric Sounding Interferometer, Clerbaux et al., 2007) are nadir viewing Fourier-transform spectrometers designed for operation on the meteorological Metop satellites (ESA/EUMETSAT). The first instrument was launched in orbit aboard the satellite Metop-A on 19 October, 2006, and started operational measurements in June 2007. Two other IASI instruments will be launched in 2010 and 2015, respectively, with a nominal lifetime of 5 years. IASI is a Michelson-type Fourier-transform spectrometer with a maximal optical path difference of 2 cm and a spectral range from 645 cm^{-1} to 2760 cm^{-1}. After apodisation with a Gaussian function, a spectral resolution of 0.5 cm^{-1} is obtained. The instrument scans the Earth's surface perpendicular to the satellite's flight track with 15 individual views on each side of the track. At the nadir point, the size of one view is 50×50 km. It consists of 4 individual ground pixels with 12 km diameter each (at the nadir point), achieved by using 4 detector pixels for each IASI channel. The maximum scan angle of 48.3 degrees from nadir equals a distance of 1100 km from the centre of the ground pixel to the flight track projection (sub-satellite point).

The polar sun-synchronous orbit of Metop crosses the equator at two fixed local solar times: 09:30 a.m. (descending) and 09:30 p.m. (ascending). The distance between two successive overpasses is 25 degrees longitude, this equals 2800 km at the equator and decreases towards the poles. For latitudes higher than 45 degrees, the scanning ranges of two successive overpasses overlap. This means that a location like Paris

ACPD
9, 11441–11479, 2009

(49° N) is covered by at least 2 overpasses per day. Depending on where these overlap regions are located, up to four overpasses can occur.

The Eumetsat products of IASI distributed by EUMETCast are surface temperature, cloud properties, vertical profiles of temperature and humidity, and partial columns of ozone and several other trace gases.

3 The different retrieval approaches

The measured spectra of IASI (or any other spectrometer) can be simulated by the use of an atmospheric radiative transfer model. Based on the radiative transfer equation, the spectral radiances that are measured by the instrument are calculated with such a model taking into account the atmospheric and instrumental parameters. A comparison of atmospheric radiances calculated with different radiative transfer models has been made previously by Tjemkes et al. (2003) with the result of a generally good agreement in the spectral range from 800–2600 cm^{-1}. The agreement of spectra calculated with radiative transfer models compared to the measured spectra depends not only on the exact implementation of the basic equations in the algorithms, but also on the atmospheric and instrumental parameters that are used in these calculations.

For the ozone retrieval of the different teams, the used temperature profiles have been derived from ECMWF and the spectroscopic data were taken from the HITRAN 2004 database (Rothman et al., 2005), except for the retrieval at LISA (see below). Here it should be also mentioned, that for the mid-latitude retrievals compared in this study, all teams use one unique a priori profile for ozone for the entire time period. This avoids differences in the retrieved profiles due to a temporally and/or spatially changing a priori profile, and demonstrates that the differences are indeed due to the measured signal.

To obtain the vertical ozone profile from a given atmospheric spectrum, the atmospheric radiative transfer model has to be inverted. There are two principal numerical approaches to perform this inversion.

The first one is a full numerical method: the atmospheric profile predicted by the radiative transfer model is iteratively adapted to minimise the (root mean squared) difference between the calculated and measured spectra. The minimisation may be constraint by the smoothness of the profile (Tikhonov-Philips regularisation, Tikhonov, 1963; Phillips, 1962), by its closeness to a given a priori profile (optimal estimation, Rodgers, 2000), or by a combination of both constraints. For each iteration step, the full radiative transfer has to be calculated. This approach is time-consuming. In the developing phase of IASI, it was not possible to perform this inversion in real time (120 spectra in 8 s) for the operational retrieval.

The second approach is a neural network: the network is trained by spectra calculated from various different atmospheric profiles with the aim of reproducing the columnar amounts. The inversion of a given spectrum with the neural network is a nonlinear interpolation of the training data set. Extreme atmospheric situations which were not covered by the training dataset may lead to wrong columns, since the network performs a nonlinear extrapolation. This problem is counterbalanced by the high calculation speed of this method. For this reason, the neural network approach was chosen for the operational data processing at EUMETSAT (Turquety et al., 2004).

In the following subsections we describe briefly the different retrieval approaches that were used in the intercomparison of the ozone products of this study with the balloon sonde profiles.

3.1 Retrieval at LATMOS

At LATMOS (Laboratoire Atmosphères, Milieux, Observations Spatiales, France), trace gases concentrations are retrieved from the IASI spectra using different algorithms (Clerbaux et al., 2009). For the ozone profiles, the ATMOSPHIT software (Clerbaux et al., 2005; Coheur et al., 2005) is used. It contains ray tracing for various geometries, a line-by-line radiative transfer model and an inversion scheme that relies on the Optimal Estimation (OE) theory (Rodgers, 2000). A synthetic spectrum is computed in ATMOSPHIT using the line parameters and absorption cross sections for the heavier

molecules, as collected in the HITRAN 2004 database. The OE retrieval approach relies on prior assumptions that determine the linearisation point about which a retrieval is constrained. This is known as a priori information, composed of a mean state and an a priori covariance matrix, which has to represent the best statistical knowledge of the state prior to the measurements. A full description of the retrieval set-up is provided in Boynard et al. (2009). Temperature profiles used in the inversion process are bi-linear interpolation of ECMWF temperature fields on the IASI observation pixels.

LATMOS retrievals cover the entire period, but have not been performed for all stations (see Table 1).

3.2 Retrieval at LISA

The retrieval of ozone profiles from IASI spectra at LISA (Laboratoire Interuniversitaire des Systèmes Atmosphériques, France) is performed with the radiative transfer model KOPRA (Karlsruhe Optimised and Precise Radiative transfer Algorithm, Stiller et al., 2000) and its numerical inversion module KOPRAFIT. KOPRA was developed for the retrieval of spectra of the MIPAS instrument aboard ENVISAT (Fischer et al., 2008). Recently it has also been applied to the analysis of spectra measured with IASI on Metop (Eremenko et al., 2008). The atmospheric profiles are calculated on a vertical grid of 1 km below 40 km and 2 km above. To achieve maximal information content in the troposphere, the regularisation was adapted to the atmospheric weighting function and the IASI viewing geometry. Here, a combination of zero, first and second order Thikonov constraints with altitude-dependent coefficients similar to Kulawik et al. (2006) was employed. These coefficients were optimised using a simplex method (Nelder and Mead, 1965) to both maximise the Degrees of Freedom (DOF) of the retrieval (Steck, 2006) in the troposphere and to minimise the total error of the retrieved profile.

The analysis of IASI data at LISA is performed in three steps (with ozone being the last step): the first step is the retrieval of effective surface temperature. Note that the radiance reaching the top of the atmosphere is not necessarily from the surface, but may be influenced by water vapour and dust or aerosol in the boundary layer. To es-

timate the background radiance, a blackbody with emissivity equal to 1 was assumed and its temperature was retrieved at 11 μm close to the ozone band used in the retrieval. In the second step, the atmospheric temperature profile is retrieved using the CO_2 band around 15 μm and the ECMWF profiles as a priori. Finally, in the third step, the ozone profile retrieval is performed in the 975–1100 cm^{-1} spectral region using seven microwindows that exclude strong water lines. For ozone, the spectroscopic parameters from the MIPAS database (Flaud et al., 2003) were used, and for all other species the data in HITRAN 2004. The a priori information was constructed using the climatology of McPeters et al. (2007).

Before all retrievals, the IASI spectra are filtered for cloud contamination, and only spectra for clear sky conditions are used in the intercomparison data set. After their retrieval, the ozone profiles are screened for nonphysical shapes. The DOF for the ozone retrievals is about 3.5, depending on the surface temperature and thermal contrast. For the calculation of the total errors, one must consider spectroscopic errors, noise errors, errors in the temperature profile and the smoothing error. The error of the profile is assumed to be between 20 and 40% (1σ), the error of the columns 1050–478.54 hPa (0–6 km), 1050–222.94 hPa (0–11 km), and 1050–132.49 hPa (0–14 km) to be between 15 and 29%, between 10 and 16%, and between 6 and 13%, respectively, depending on the surface temperature (the error is larger for a colder surface and for a weaker thermal contrast) and the ozone mixing ratios.

For more details on the retrieval, especially on regularisation and error estimation, the reader should refer to Eremenko et al. (2008).

LISA retrievals cover the entire period and all stations listed in Table 1.

3.3 Retrieval at LPMAA

LPMAA (Laboratoire de Physique Moléculaire pour l'Atmosphère et l'Astrophysique, France) Atmospheric Retrieval Algorithm (LARA) which has been developed over the years is a home made radiative transfer model associated with an inversion algorithm. The corresponding software has been used to analyse atmospheric spectra recorded

using ground-based, balloon- or satellite-borne experiments, both in absorption or emission mode, and for the limb or nadir geometry. LARA has been used to perform simulations of atmospheric spectra for the preparation of satellite experiments and for assessing the information content expected from instruments with different characteristics.

The algorithm LARA allows the simultaneous inversion of spectra in several windows for the joint retrieval of vertical profiles (or slant column densities) of various species (Payan et al., 1998). Surface temperature and emissivity, and if needed instrumental line shape or instrumental spectral shift may be fitted together with the species.

The LPMAA retrieval algorithm includes an accurate line-by-line radiative transfer model and an efficient minimisation algorithm of the Levenberg-Marquardt type. The optimal estimation method is used for the retrieval process. The full error covariance matrix is calculated within the retrieval process. The forward model (i.e. the radiative transfer model) uses molecular parameters which are mainly extracted from the HITRAN 2004 database. Individual line shapes are calculated with a Voigt profile based on the Lorentzian parameters listed in the spectroscopic database and the line shifting coefficient can be used when non-zero in HITRAN 2004. The calculation is accounting for the water vapour continuum (Clough et al., 2005) as well as water vapour self-broadening. The reflected downward flux and the reflected or diffused sunlight are modelled.

For the present work, the algorithm was tailored to the specificities of the IASI spectra and geometry. Surface emissivity has been fixed to one, while surface temperature has been retrieved together with the ozone profile.

LPMAA retrievals cover summer (JJA) 2007 and three European mid-latitude stations (see Table 1).

3.4 Retrieval at EUMETSAT

The neural network used for ozone at EUMETSAT is of feed-forward type with two hidden layers. From selected channels in the input layer it derives 4 partial ozone columns

in the output layer. The partial columns span 1050–478.54 hPa, 1050–222.94 hPa, 1050–132.49 hPa, and 1050–0.005 hPa, respectively. The two first columns cover only the troposphere, whereas the last one is the total column. We refer to Turquety et al. (2004) for more details. The target accuracy for the partial columns was set to 28%, 15%, 9%, and 2.5%, respectively for cloud-free conditions. The algorithm is able to treat optically thin clouds, nevertheless concerned columns are flagged. We decided to exclude columns flagged as (partially) cloudy in the comparison, to avoid the question, whether differences in the ozone columns derive from the ozone or the cloud treatment.

Ozone columns are available from 26 February 2008 ongoing, but only for pixels with odd numbers. The ozone total column is about 30 Dobson Units (DU) until the morning overpass on 10 June, 2008. For these data, for intercomparison, we scaled all four columns by a factor 10. Ongoing from the evening of 10 June 2008, the total columns show the expected values of about 300 DU. Until 11 August 2008, the retrieval version was v4.2, the successive version v4.3 was trained with a new data set. We limited therefore the comparison on version v4.2. Until now, for the validation of v4.3, there are not enough sonde measurements available.

In the case of low thermal contrast between the surface and the lowest layer of the atmosphere, the ozone in the first 1–2 km does not give a signature in the top of the atmosphere spectra. This "hidden" part of the profile is treated differently by the particular retrieval approaches. The retrieval with a neural network is more or less the selection of the best matching profile from the training dataset. The profile in the hidden part is selected by use of the visible part. The constraint of the numerical inversion makes the retrieved profile fall back onto the a priori information for those parts of the atmosphere, where the measurement is not sensitive. The a priori information is the same for all retrievals and does not depend on the actual profile. A Thikonov regularisation constrains the deviation of the profile not its value – in this case, the profile is continued down to surface with the same shape as the a-priori profile.

ACPD
9, 11441–11479, 2009

4 Ozone sonde profiles

Ozone sondes are in-situ instruments which are taken from ground up to the stratosphere (35 km) by a rubber balloon filled with hydrogen. Besides of the electrochemical ozone sensor, most sondes are equipped with GPS (for altitude information) and with temperature and humidity sensors. The high vertical resolution of the measured profiles of about 5 m is reduced in the stored files to 250 m for most sondes. The accuracy of the measured ozone concentrations is quoted as about ±(5–10)% (Deshler et al., 2008; Smit et al., 2007; Thompson et al., 2003). A major error source is related to the pump-flow dependence on outside pressure. To quantify this error contribution, the ozone total column calculated from the measured ozone profiles is compared with a nearby UV-spectrometer measurement, either ground-based or satellite-based. All Japanese, German, and Belgian ozone sonde profiles are multiplied with a correction-factor (CF), defined as the ratio of the two columns.

As the error in the pump-flow increases for low pressures, this method corrects the stratospheric values but may degrade the tropospheric values (Smit et al., 2007). In the present paper, both types of sonde data were used: "corrected" and "uncorrected" ones. No selection of the "uncorrected" sonde profiles due to the correction-factor was made, because the discrepancies between the two columns should mainly occur in the stratosphere. Only sonde profiles that were corrected by more than 15% were rejected since this large correction may also have affected the tropospheric values.

Because the sondes never reach the top of the atmosphere, an assumption for the remaining part of the profile has to be made to calculate the ozone total column. In the literature (as in the used ozone sonde data), two different approaches are reported: the extrapolation of the profile based on constant mixing ratio (CMR), or the use of the SBUV satellite climatology of McPeters et al. (2007). The advantage of the first method is the individual treatment of each sonde, whereas the second method may be more accurate on average (Thompson et al., 2003). If the sonde data already includes a total column estimate this value was used here, but in case the ozone total column was not

given, the CMR method was used. For sonde data where the correction factor was not given, it was calculated from the comparison with daily assimilated (Level-3) columns of the Ozone Monitoring Instrument (OMI) aboard the NASA EOS-Aura satellite, which are available at ftp://toms.gsfc.nasa.gov/pub/omi/data/ozone. In Table 1 we give the averaged correction-factor for each sonde station.

For the sondes used here, three different types of ozone sensors are employed. Most sondes use electrochemical concentration cells (ECC), which measure the oxidation of a potassium iodide (KI) solution by the ozone in the ambient air. The Japanese sondes utilise modified electrochemical concentration cells with carbon anodes (carbon-iodine, KC). The profiles of these KC-sondes are always corrected by a nearby UV-measured total column. The ozone sondes launched at Hohenpeißenberg are equipped with Brewer-Mast (BM) sensors, which are also based on the oxidation of potassium iodide. As for the Japanese sondes, the profiles at Hohenpeißenberg and the profiles at Uccle and Lindenberg (both ECC sensors) are always corrected with a nearby total column measurement. The profiles of the other sondes are left unchanged. A more detailed description of the ozone sonde principles can be found at http://www.fz-juelich.de/icg/icg-2/josie/ozone_sondes/.

The sondes used in this paper are taken from three archives, namely (1) the World Ozone and Ultraviolet Data Center (WOUDC) (http://www.woudc.org), (2) the Global Monitoring Division (GMD) of NOAA's Earth System Research Laboratory (http://www.esrl.noaa.gov/gmd), and (3) NILU's Atmospheric Database for Interactive Retrieval (NADIR) at Norsk Institutt for Luftforskning (NILU) (http://www.nilu.no/nadir/).

5 Selection criteria

The dense spatial coverage of IASI gives us the possibility to use a rather tight coincidence criterium: the footprints of the compared profiles must be inside a square of ±110 km side length (±1 degree latitude) around the sonde station. On the contrary, the low frequency of overpasses (two per day) leads to a relatively loose temporal over-

lap criterium: the time of the IASI measurement must be within 12 h from the sonde measurement. Note that both these criteria are in agreement with the wide range of coincidence criteria found in the literature (Cortesi et al., 2007; Dupuy et al., 2009; Nassar et al., 2008). The number of spectra that fulfill the coincidence criteria for one overpass can reach 26 (for a nadir angle of zero degree).

Besides the coincidence with the ozone sonde, IASI spectra that were used in the comparisons presented below had to fulfill other criteria as well: first of all, only spectra were used that passed the cloud-filter (different for all teams). Also, only spectra with nadir angles lower than 32 degree were used to produce equal databases for all retrieval approaches involved. Finally, the number of selected spectra were limited to 9 per coincidence, since this gives a sufficient statistic and reduces computation time. If more than 9 spectra passed all filters, those with the highest surface temperatures were selected. These spectra show typically the best thermal contrast. To have sufficient statistics, only coincidences with four or more spectra passing all filters were used.

The selection of ozone sondes here is limited on those stations where profiles were available for the entire validation period. However, the number of stations in the tropics is very limited and for the existing profiles, the coincident IASI spectra are strongly affected by clouds. We therefore decided to concentrate the present study on northern mid-latitudes (30° N–70° N latitude). Table 1 gives a summary of all sounding stations, their location, some details on the measurements, and the number of coincidences.

6 Comparison methodology

In this section we describe the comparison between the ozone profiles from IASI (retrieved by several teams) with the profiles measured by balloon sondes (that are assumed to be a good estimate of the real state of the atmosphere). We also introduce the derivation of column amounts from the in-situ measured and remotely sensed (IASI) profiles.

Following the formalism of Rodgers (2000), the retrieved profile is $\hat{z}$:

$$\hat{z} = x_a + \mathbf{A}(x - x_a) + \epsilon_z \quad (1)$$

with x the true state of the atmosphere, $\mathbf{A}$ the averaging kernel matrix, and x_a the a priori profile. The term ϵ_z sums all errors due to the forward model, the linearisation of the problem and the measurement.

The profile x_s measured by the balloon sondes consists of the true atmospheric profile x and a measurement error ϵ_s.

$$x_s = x + \epsilon_s \quad (2)$$

We compare now the balloon sonde profile x_s with the retrieved IASI profile $\hat{z}$. We find, that the difference ($\hat{z}$–x_s) contains not only error terms, but is strongly dependent also on the atmospheric profile, the a-priori assumptions and the averaging kernel. To get rid of this unlucky dependency, we transform the sonde measurement in a pseudo retrieved profile $\hat{x}$ similar to Eq. (1).

$$\hat{x} = x_a + \mathbf{A}(x_s - x_a) \quad (3)$$

The difference between the pseudo retrieved profile $\hat{x}$ and the retrieved profile $\hat{z}$ is an error term, containing only the errors in the retrieval ϵ_z and the errors in the sonde measurement ϵ_s.

$$\begin{aligned} \hat{z} - \hat{x} &= (x_a + \mathbf{A}(x - x_a) + \epsilon_z) - (x_a + \mathbf{A}(x + \epsilon_s - x_a)) \quad (4) \\ &= \epsilon_z - \mathbf{A}\epsilon_s \end{aligned}$$

Making the average over a large number of comparisons separates this error term in its systematic and its random part. The average is an estimate for the systematic error, whereas the standard deviation is an estimate for the random error.

The comparison of volume mixing ratio profiles (see Figs. 2a, b, 3a, b) is performed on the individual retrieval grid of the teams.

For the comparison of the "tropospheric" columns, we integrated the pseudo retrieved profile $\hat{\boldsymbol{x}}$ from the surface up to 222.94 hPa to create the sonde column. The retrieved profile was also integrated from the surface up to 222.94 hPa to give the IASI-column. The same steps were performed for the columns from the surface up to 478.54 hPa and 132.49 hPa.

For the comparison with the results of the neural network at EUMETSAT, no a priori profiles or averaging kernels are available. But as the network was trained to reproduce the real column amounts from the surface up to 222.94 hPa, we compared the retrieved columns with the integrated raw sonde profile also from the surface up to 222.94 hPa. We similarly calculated the columns from the surface up to 478.54 hPa and 132.49 hPa.

6.1 Grid change from the fine sonde grid to the coarse retrieval grid

The retrievals are performed on a coarse grid, compared to the sonde measurement. Therefore one cannot use the raw sonde measurement $\boldsymbol{x}_S$ for $\boldsymbol{x}$ in Eq. (1). Following Rodgers (2000) we best approximate the sonde using Eq. (5).

$$\boldsymbol{x} = \left(\mathbf{W}^{\mathbf{t}}\mathbf{W}\right)^{-1}\mathbf{W}^{\mathbf{t}}\boldsymbol{x}_S \tag{5}$$

where $\boldsymbol{x}_S$ is the measured sonde profile and $\mathbf{W}$ is the operator for linear interpolation from the coarse retrieval grid to the finer sonde grid. The left side term $\boldsymbol{x}$ in Eq. (5) is an optimal approximated sonde profile.

6.2 The averaging kernels of LATMOS, LISA, and LPMAA

The averaging kernels (i.e. the rows of the averaging kernel matrix A) reflect the sensitivity of the retrieved profiles on the true state of the atmosphere. The choice of the retrieval approach can slightly modify the sensitivity, but not the general characteristics of the inversion and of the averaging kernel matrix. In Fig. 1 we show the diagonals of typical averaging kernel matrices for the different retrieval methods involved in this work. To make the values comparable, we transformed the averaging kernel matrix of

ACPD
9, 11441–11479, 2009

the LISA and LPMAA retrievals onto the LATMOS-grid, using Eq. (6) (von Clarmann and Grabowski, 2007):

$$\tilde{\mathbf{A}} = \left(\mathbf{W}^t\mathbf{W}\right)^{-1}\mathbf{W}^t\mathbf{A}\mathbf{W} \quad (6)$$

where **A** is the averaging kernel matrix on the original (finer) grid and **W** is the operator for linear interpolation from the coarse grid to the finer grid. The left side term $\tilde{\mathbf{A}}$ in Eq. (6) is an optimal approximated averaging kernel matrix. Figure 1 illustrates the high sensitivity of all retrievals in the lower stratosphere and upper troposphere, and the weaker sensitivity in the lowest part of troposphere especially near the surface. An adapted retrieval approach can increase this weak sensitivity in the lower troposphere, the DOF for the tropospheric column from the surface up to 11 km are significantly higher for LISA (1.2–1.5) than for LATMOS (0.5–0.9) and LPMAA (0.4). The Figure also illustrates the dependence of the retrieval sensitivity on surface temperature.

7 Results

In this section we describe the comparison between the remotely sensed ozone-profiles and tropospheric columns (IASI) with the in-situ measured data (balloon sondes). The comparison is threefold: (1) we compare mean profiles for individual sonde stations with the coincident mean IASI retrieved profiles, (2) we compare the individual IASI partial columns with their sonde equivalent, and (3) we investigate the statistical distribution of the difference between IASI and sonde partial columns.

7.1 Comparison of mean profiles

In Fig. 2a we show the mean profiles retrieved at LATMOS, LISA, and LPMAA together with the mean sonde measurements for three selected European sonde locations. We also give the mean sonde profiles convolved with the averaging kernels – the expected retrieved profiles $\hat{\boldsymbol{x}}$ using Eq. (3). The averages are performed over the summer period

2007, using coincidences which are cloud-free for all three teams (the columns show LATMOS, LISA, and LPMAA, from left to right). For each retrieved profile we use the corresponding averaging kernels and a priori profiles. Figure 2b shows the differences between the retrieved profiles and the sonde profiles or the convolved sonde profiles, respectively. Here we give also the variability (1σ) of the difference between the retrieved profile and the convolved sonde profile as bars. Both Figures show the similarity of the retrieved profiles to the convolved sonde profiles, i.e. the mean retrieval error is small (less than 0.02 ppmv below 10 km for LATMOS and LISA, less than 0.04 ppmv for LPMAA). The Figure shows the effect of convolution of the sonde profile with the averaging kernels. In the case of LISA, the convolved sonde profile stays close to the raw profile, whereas in the case of LATMOS, the convolution introduces a small but visible difference (about 0.01 ppmv). In the case of LPMAA, the effect of the convolution is even larger. This may be explained by the weaker sensitivity of LATMOS and LPMAA in the lower troposphere, what leads the convolved profile towards the a priori. This may also partly explain the lower variability of the LATMOS retrievals compared to LISA retrievals. In Fig. 3a and b we give the mean profiles for the whole validation period (6.2007–8.2008) together with the differences for all mid-latitude ozone sondes processed by LATMOS and LISA. Again the comparison shows the good quality of the retrieved profiles.

For the retrievals made at LATMOS and LISA the convolution does not affect so much the sonde profile, the retrieved profiles are also close to the raw sonde profiles. The retrieved profiles are a good estimation of the atmospheric profile. Though, for scientific use, e.g. in chemical models or assimilation, one should be aware of the altitude dependent sensitivity, expressed in the averaging kernels.

7.2 Comparison of individual partial columns

To investigate the quality of the individual profiles, we compared the "tropospheric" ozone columns of the different retrievals and the sonde measurements. The tropospheric columns here are defined as the column from the surface up to 223 hPa (about

0–11 km) and 478.54 hPa (about 0–6 km), respectively. We have chosen the tropospheric levels that are available for the EUMETSAT retrieval. The degrees of freedom for the higher column are about one. In Fig. 4 we compare the columns retrieved at LATMOS and at LISA with sonde columns for the mid-latitude stations processed by LATMOS (see Table 1), and for the time period from June 2007 to August 2008. The Figure shows the high quality of the retrieval results for both teams. The Figure also shows the effect of the sonde profile convolution on the comparison quality. Especially in the case of the retrieval performed at LATMOS, the comparison with the convolved sonde profiles shows a lower variability and a higher correlation coefficient than the comparison with the raw sonde profiles. Also the slope is closer to unity and the intercept is closer to zero. These effects due to the convolution are less pronounced for the retrieval at LISA. The correlation coefficient obtained with the LISA product is slightly smaller when the convolution is applied compared to the LATMOS product but the slope is always closer to unity.

7.3 Statistical comparison of partial columns

We also studied the distribution of the partial column differences between the retrievals and the sonde measurements. Figure 5 shows histogram plots for the retrievals of mid-latitude coincidences performed at LATMOS and LISA for the period from June 2007 to August 2008, and for the retrievals at EUMETSAT and LISA for the EUMETSAT v4.2 period from February 2008 to August 2008. We included all IASI profiles in the statistic, which have been processed by the individual teams and passed their cloud-filters. No averaging kernels and a priori profiles are available for the neural network retrieval performed by EUMETSAT. Because we want to show equal treatment of all retrievals, we have made no convolution of the sonde measurement. We summarised the statistical parameters in Table 2, here we give also the parameters for differences to the convolved sonde profiles.

Besides the retrieval error and the measurement error of the sondes, the difference between the raw sonde and the retrieved profiles also contains an a priori error. As

ACPD
9, 11441–11479, 2009

can be seen from the statistics in Table 2, this a priori error changes the bias (the systematic error estimate) and the standard deviation (the estimate for the random errors) of the distribution. This effect is more pronounced for the retrievals performed at LATMOS than for those of LISA. The retrieval at LATMOS shows a bias of 0.3 DU for the comparison of the 0–6 km column with the convolved sonde, whereas the comparison with the raw sonde leads to a bias of 3.5 DU. The variability changes from 6.1% to 17.7% for the same example. The bias of the LISA retrieval is less than 1.5 DU in both cases and the variability is slightly larger than for the LATMOS, it changes from 18% to 24.1%.

Nevertheless, the retrievals at LATMOS and LISA have small biases for the tropospheric columns (less than 2 DU), and the variability equals the expected error budget. In contrast, the retrieval at EUMETSAT shows a high bias of about 5 DU for the two tropospheric columns. This is in agreement with the validation study made by Oduleye et al. (2008), but greater than the target accuracy. We limited the comparison with LISA retrievals on the same period as the comparison with EUMETSAT (4th line in Table 2), to exclude seasonal effects or other problems taking place only in this special time. The retrieval at LISA shows the same random error distribution, but a much lower bias than EUMETSAT. Both bias and variability of LISA are in agreement with the results for the entire period. The comparison of the columns from the surface up to 14 km shows a similar quality of the EUMETSAT, LATMOS, and LISA retrievals with a bias of about 3 DU and a variability of about 16%.

To test the dependency on seasonal atmospheric variations, we made individual histograms for the columns from the surface up to 11 km for the four seasons (see Fig. 6). The retrieval at LISA has a small dependency on the seasons, with small but varying biases and standard deviations being a little bit higher in winter and spring than in summer and autumn. Interpreting the bias as expectation value of a normal-distribution, the associated error (e.g. for DJF) is $\sigma_\mu = \sigma/\sqrt{n} = 8.5/\sqrt{194} = 0.6$. This may partly explain the variability of the biases.

ACPD
9, 11441–11479, 2009

7.4 Climatology of LISA partial columns

In Fig. 7 we show all the individual columns (LISA retrievals and unconvolved sonde measurements, red and blue symbols) grouped in months and latitude bands as in the Labow, Logan, McPeters (LLM) climatology (McPeters et al., 2007). We give also the monthly means (coloured lines), the column of the a priori profile (dashed black line), and the climatological means with their variability (3σ, black line with bars). Note in particular that the retrievals at LISA are not sticking at the constant a priori and reproduce well the annual variation of ozone in the mid-latitudes. The dispersion of the retrieved value for each month is consistent with the variability prescribed by the climatology.

8 Conclusions

In this study we have compared the IASI ozone retrieval of several teams to a large set of ozone sondes profiles at mid-latitudes. The goal was to quantify the systematic and the random errors of the different algorithms. The difference of the retrieved profiles to the sondes profiles contains three kinds of errors: the measurement error of the ozone sonde (5–10%), the retrieval error (20–40%) and the error of the a priori profile. The application of the retrieval operator to the sonde profile prior to the difference eliminates the a priori error. In the case of the retrieval at LISA the a priori error is quite small (less than 1 DU in average, for all partial columns). Compared to the retrieval at LISA, the stronger regularisation of the retrieval at LATMOS leads to a smaller variability in the comparison with the convolved sonde profiles (e.g. 6.1% instead of 17.7%, for the columns 0–6 km), but to a higher bias in the comparison with the raw sondes (e.g. 3.5 DU instead of 0.3 DU, also for the columns 0–6 km). The systematic bias of the retrieval at LISA shows a small dependency on the season, whereas the bias is generally small (less than 3 DU for the columns from the surface up to 223 hPa). The variability (17.8% for the columns from the surface up to 223 hPa) is consistent with the

ACPD
9, 11441–11479, 2009

upper bound of the estimated combined error (11–19%) of the retrieval (10–16%) and the sonde (5–10%). For the compared cases, the profile retrievals at LATMOS show no significant differences to the retrieval at LISA. This demonstrates that the achievable retrieval quality, which is limited by atmospheric and instrumental properties, is obtained for these retrievals. The retrieval at EUMETSAT is still in a pre-operational developing phase, in this study we compared the v4.2 version, which was applied to the data until 11 August 2008. The EUMETSAT tropospheric columns are higher than the sonde columns by more than 5 DU on average with a variability of about 20%, this is slightly worse than the target accuracy. The EUMETSAT columns from the surface up to 14 km show a similar quality to LATMOS and LISA retrievals with a bias of about 3 DU and a variability of about 17%. EUMETSAT changed the training of the neural network (August et al., 2008) to enhance the retrieval quality. The validation of the subsequent version v4.3 (in use until January 2009) is an ongoing process and can not be presented in this study due to the insufficient number of available sonde data for this period.

Acknowledgements. IASI has been developed and built under the responsibility of the Centre National d'Etudes Spatiales (CNES, France). It is flown aboard the Metop satellites as part of the EUMETSAT Polar System. The IASI L1C and L2 data have been received through the EUMETCast near real time data distribution service and provided by the Ether French atmospheric database (http://ether.ipsl.jussieu.fr). The presented study has been supported by CNES in the frame of the IASI-TOSCA project. The temperature and altitude fields have been taken from ECMWF, and the ozone total columns of OMI from NASA (ftp://toms.gsfc.nasa.gov/pub/omi/data/ozone/). The ozone sonde data have been taken from the following archives: the World Ozone and Ultraviolet Data Center (WOUDC) (http://www.woudc.org), the Global Monitoring Division (GMD) of the Earth System Research Laboratory (http://www.esrl.noaa.gov/gmd), and the NILU's Atmospheric Database for Interactive Retrieval (NADIR) at Norsk Institutt for Luftforskning (NILU) (http://www.nilu.no/nadir/). Since June 2007 funding from the Environmental Protection Agency (EPA, Reference Number: 2006-AQ-MS-50) has allowed Valentia Observatory to extend its Ozonesonde launches to a year round weekly programme. The authors want to thank all the above mentioned institutions for their helpful work. We want to thank also the colleagues for launching sondes in Legionowo and Uccle.

The publication of this article is financed by CNRS-INSU.

References

August, T., Schlüssel, P., Munro, R., Calbet, X., Oduleye, O., Arriaga, A., Hultberg, T., Hadji-Lazaro, J., Turquety, S., and Clerbaux, C.: ANN ozone retrieval within the operational IASI level 2 processor, in: Proceedings of the 2008 EUMETSAT meteorological satellite conference, Darmstadt, Germany, 8–12 September, 2008. 11462

Boynard, A., Clerbaux, C., Coheur, P.-F., Hurtmans, D., Turquety, S., George, M., Hadji-Lazaro, J., Keim, C., and Meyer-Arnek, J.: Measurements of total and tropospheric ozone from IASI: comparison with correlative satellite and ozonesonde observations, Atmos. Chem. Phys. Discuss., 9, 10513–10548, 2009, http://www.atmos-chem-phys-discuss.net/9/10513/2009/. 11448

Clerbaux, C., Coheur, P.-F., Hurtmans, D., Barret, B., Carleer, M., Colin, R., Semeniuk, K., McConnell, J. C., Boone, C., and Bernath, P.: Carbon monoxide distribution from the ACE-FTS solar occultation measurements, Geophys. Res. Lett., 32, L16S01, doi:10.1029/2005GL022394, 2005. 11447

Clerbaux, C., Hadji-Lazaro, J., Turquety, S., George, M., Coheur, P.-F., Hurtmans, D., Wespes, C., Herbin, H., Blumstein, D., Tournier, B., and Phulpin, T.: The IASI/MetOp I mission: First observations and highlights of its potential contribution to GMES, Space Res. Today, 168, 19–24, 2007. 11445

Clerbaux, C., Boynard, A., Clarisse, L., George, M., Hadji-Lazaro, J., Herbin, H., Hurtmans, D., Pommier, M., Razavi, A., Turquety, S., Wespes, C., and Coheur, P.-F.: Monitoring of atmospheric composition using the thermal infrared IASI/MetOp sounder, Atmos. Chem. Phys.

Discuss., 9, 8307–8339, 2009, http://www.atmos-chem-phys-discuss.net/9/8307/2009/. 11447
Clough, S. A., Shephard, M. W., Mlawer, E. J., Delamere, J. S., Iacono, M. J., Cady-Pereira, K., Boukabara, S., and Brown, P. D.: Atmospheric radiative transfer modeling: a summary of the AER codes, Short Communication, J. Quant. Spectrosc. Ra., 91, 233–244, 2005. 11450
Coheur, P.-F., Barret, B., Turquety, S., Hurtmans, D., Hadji-Lazaro, J., and Clerbaux, C.: Retrieval and characterization of ozone vertical profiles from a thermal infrared nadir sounder, J. Geophys. Res., 110, D24303, doi:10.1029/2005JD005845, 2005. 11444, 11447
Cortesi, U., Lambert, J. C., De Clercq, C., Bianchini, G., Blumenstock, T., Bracher, A., Castelli, E., Catoire, V., Chance, K. V., De Maziére, M., Demoulin, P., Godin-Beekmann, S., Jones, N., Jucks, K., Keim, C., Kerzenmacher, T., Kuellmann, H., Kuttippurath, J., Iarlori, M., Liu, G. Y., Liu, Y., McDermid, I. S., Meijer, Y. J., Mencaraglia, F., Mikuteit, S., Oelhaf, H., Piccolo, C., Pirre, M., Raspollini, P., Ravegnani, F., Reburn, W. J., Redaelli, G., Remedios, J. J., Sembhi, H., Smale, D., Steck, T., Taddei, A., Varotsos, C., Vigouroux, C., Waterfall, A., Wetzel, G., and Wood, S.: Geophysical validation of MIPAS-ENVISAT operational ozone data, Atmos. Chem. Phys., 7, 4807–4867, 2007, http://www.atmos-chem-phys.net/7/4807/2007/. 11454
Deshler, T., Mercer, J. L., Smit, H. G. J., Stubi, R., Levrat, G., Johnson, B. J., Oltmans, S. J., Kivi, R., Thompson, A. M., Witte, J., Davies, J., Schmidlin, F. J., Brothers, G., and Sasaki, T.: Atmospheric comparison of electrochemical cell ozonesondes from different manufacturers, and with different cathode solution strengths: The Balloon Experiment on Standards for Ozonesondes, J. Geophys. Res., 113, D04307, doi:10.1029/2007JD008975, 2008. 11452
Dupuy, E., Walker, K. A., Kar, J., Boone, C. D., McElroy, C. T., Bernath, P. F., Drummond, J. R., Skelton, R., McLeod, S. D., Hughes, R. C., Nowlan, C. R., Dufour, D. G., Zou, J., Nichitiu, F., Strong, K., Baron, P., Bevilacqua, R. M., Blumenstock, T., Bodeker, G. E., Borsdorff, T., Bourassa, A. E., Bovensmann, H., Boyd, I. S., Bracher, A., Brogniez, C., Burrows, J. P., Catoire, V., Ceccherini, S., Chabrillat, S., Christensen, T., Coffey, M. T., Cortesi, U., Davies, J., De Clercq, C., Degenstein, D. A., De Maziére, M., Demoulin, P., Dodion, J., Firanski, B., Fischer, H., Forbes, G., Froidevaux, L., Fussen, D., Gerard, P., Godin-Beekmann, S., Goutail, F., Granville, J., Griffith, D., Haley, C. S., Hannigan, J. W., Höpfner, M., Jin, J. J., Jones, A., Jones, N. B., Jucks, K., Kagawa, A., Kasai, Y., Kerzenmacher, T. E., Kleinböhl, A., Klekociuk, A. R., Kramer, I., Küllmann, H., Kuttippurath, J., Kyrölä, E., Lambert, J.-C., Livesey, N. J., Llewellyn, E. J., Lloyd, N. D., Mahieu, E., Manney, G. L., Marshall, B. T., McConnell, J. C.,

McCormick, M. P., McDermid, I. S., McHugh, M., McLinden, C. A., Mellqvist, J., Mizutani, K., Murayama, Y., Murtagh, D. P., Oelhaf, H., Parrish, A., Petelina, S. V., Piccolo, C., Pommereau, J.-P., Randall, C. E., Robert, C., Roth, C., Schneider, M., Senten, C., Steck, T., Strandberg, A., Strawbridge, K. B., Sussmann, R., Swart, D. P. J., Tarasick, D. W., Taylor, J. R., Tétard, C., Thomason, L. W., Thompson, A. M., Tully, M. B., Urban, J., Vanhellemont, F., Vigouroux, C., von Clarmann, T., von der Gathen, P., von Savigny, C., Waters, J. W., Witte, J. C., Wolff, M., and Zawodny, J. M.: Validation of ozone measurements from the Atmospheric Chemistry Experiment (ACE), Atmos. Chem. Phys., 9, 287–343, 2009, http://www.atmos-chem-phys.net/9/287/2009/. 11454

Eremenko, M., Dufour, G., Foret, G., Keim, C., Orphal, J., Beekmann, M., Bergametti, G., and Flaud, J.-M.: Tropospheric ozone distributions over Europe during the heat wave in July 2007 observed from infrared nadir spectra recorded by IASI, Geophys. Res. Lett., 35, L18805, doi:10.1029/2008GL034803, 2008. 11444, 11448, 11449

Fischer, H., Birk, M., Blom, C., Carli, B., Carlotti, M., von Clarmann, T., Delbouille, L., Dudhia, A., Ehhalt, D., Endemann, M., Flaud, J. M., Gessner, R., Kleinert, A., Koopman, R., Langen, J., López-Puertas, M., Mosner, P., Nett, H., Oelhaf, H., Perron, G., Remedios, J., Ridolfi, M., Stiller, G., and Zander, R.: MIPAS: an instrument for atmospheric and climate research, Atmos. Chem. Phys., 8, 2151–2188, 2008, http://www.atmos-chem-phys.net/8/2151/2008/. 11448

Fishman, J., Ramanathan, V., Crutzen, P. J., and Liu, S. C.: Tropospheric ozone and climate, Nature, 282, 818–820, 1979. 11443

Fishman, J., Wozniak, A. E., and Creilson, J. K.: Global distribution of tropospheric ozone from satellite measurements using the empirically corrected tropospheric ozone residual technique: Identification of the regional aspects of air pollution, Atmos. Chem. Phys., 3, 893–907, 2003, http://www.atmos-chem-phys.net/3/893/2003/. 11444

Flaud, J.-M., Piccolo, C., Carli, B., Perrin, A., Coudert, L. H., Teffo, J.-L., and Brown, L. R.: Molecular line parameters for the MIPAS (Michelson Interferometer for Passive Atmospheric Sounding) experiment, Atmos. Ocean. Opt., 16, 172–182, 2003. 11449

Jones, D. B. A., Bowman, K. W., Horowitz, L. W., Thompson, A. M., Tarasick, D. W., and Witte, J. C.: Estimating the summertime tropospheric ozone distribution over North America through assimilation of observations from the Tropospheric Emission Spectrometer, J. Geophys. Res., 113, D18307, doi:10.1029/2007JD009341, 2008. 11444

Kulawik, S. S., Osterman, G., Jones, D. B. A., and Bowman, K. W.: Calculation of Altitude-Dependent Tikhonov Constraints for TES Nadir Retrievals, IEEE T. Geosci. Remote, 44, 1334–1342, 2006. 11448

Liu, X., Chance, K. V., Sioris, C. E., Spurr, R. J. D., Kurosu, T. P., Martin, R. V., and Newchurch, M. J.: Ozone profile and tropospheric ozone retrievals from Global Ozone Monitoring Experiment: Algorithm description and validation, J. Geophys. Res., 110, D20307, doi:10.1029/2005JD006240, 2005. 11444

McPeters, R. D., Labow, G. J., and Logan, J. A.: Ozone climatological profiles for satellite retrieval algorithms, J. Geophys. Res., 112, D05308, doi:10.1029/2005JD006823, 2007. 11449, 11452, 11461, 11479

Nassar, R., Logan, J. A., Worden, H. M., Megretskaia, I. A., Bowman, K. W., Osterman, G. B., Thompson, A. M., Tarasick, D. W., Austin, S., Claude, H., Dubey, M. K., Hocking, W. K., Johnson, B. J., Joseph, E., Merrill, J., Morris, G. A., Newchurch, M., Oltmans, S. J., Posny, F., Schmidlin, F. J., Vömel, H., Whiteman D. N., and Witte, J. C.: Validation of Tropospheric Emission Spectrometer (TES) Nadir Ozone Profiles Using Ozonesonde Measurements, J. Geophys. Res., 113, D15S17, doi:10.1029/2007JD008819, 2008. 11454

Nelder, J. A. and Mead, R.: A simplex-method for function minimization, Comput. J., 7, 308–313, 1965 11448

Oduleye, O., August, T., Calbet, X., Schlüssel, P., Arriaga, A., Hultberg, T., Aulamo, O., Kivi, R., Stiller, B., and Barfus, K.: ASI EOF and ANN Retrieved Total Columnar Amounts Ozone, Compared to Ozone Sonde and Brewer Spectrometer Measurements from the Lindenberg and Sodankylä Validation Campaigns, in: Proceedings of the 2008 EUMETSAT meteorological satellite conference, Darmstadt, Germany, 8–12 September, 2008. 11460

Payan, S., Camy-Peyret, C., Jeseck, P., Hawat, T., Durry, G., and Lefèvre, F.: First direct simultaneous HCl and ClONO2 profile measurements in the Artic vortex, Geophys. Res. Lett., 25(14), 2663–2666, 1998. 11450

Phillips, C.: A Technique for the Numerical Solution of Certain Integral Equations of the First Kind, J. Assoc. Comput. Mach., 9, 84–97, 1962. 11447

Rodgers, C. D.: Inverse Methods for Atmospheric Sounding: Theory and Practice, World Scientific Publications, Series on Atmospheric, Oceanic and Planetary Physics, Vol. 2, Singapore, 2000. 11447, 11455, 11456

Rothman, L. S. , Jacquemart, D., Barbe, A., Chris Benner, D., Birk, M., Brown, L. R., Carleer, M. R., Chackerian Jr., C., Chance, K., Coudert, L. H., Dana, V., Devi, V. M., Flaud, J.-M.,

Gamache, R. R., Goldman, A., Hartmann, J.-M., Jucks, K. W., Maki, A. G., Mandin, J.-Y., Massie, S. T., Orphal, J., Perrin, A., Rinsland, C. P., Smith, M. A. H., Tennyson, J., Tolchenov, R. N., Toth, R. A., Vander Auwera, J., Varanasi, P., and Wagner, G.: The HITRAN 2004 molecular spectroscopic database, J. Quant. Spectrosc. Ra., 96, 139–204, 2005. 11446

Seinfeld, J. H. and Pandis, S. N.: Atmospheric Chemistry and Physics, from Air Pollution to Climate Change, John Wiley & Sons Inc., Toronto, Canada, 1997. 11443

Smit, H. G. J., Straeter, W., Johnson, B., Oltmans, S., Davies, J., Tarasick, D. W., Hoegger, B., Stubi, R., Schmidlin, F., Northam, T., Thompson, A., Witte, J., Boyd, I., and Posny, F.: Assessment of the performance of ECC-ozonesondes under quasi-flight conditions in the environmental simulation chamber: Insights from the Juelich Ozone Sonde Intercomparison Experiment (JOSIE), J. Geophys Res., 112, D19306, doi:10.1029/2006JD007308, 2007. 11452

Steck, T.: Methods for determining regularization for atmospheric retrieval problems, Appl. Optics, 41, 1788–1797, 2002. 11448

Stiller, G. P. (ed) with contributions from v. Clarmann, T., Dudhia, A., Echle, G., Funke, B., Glatthor, N., Hase, F., Höpfner, M., Kellmann, S., Kemnitzer, H., Kuntz, M., Linden, A., Linder, M., Stiller, G. P., and Zorn, S.: The Karlsruhe Optimized and Precise Radiative Transfer Algorithm (KOPRA), vol. FZKA 6487 of Wissenschaftliche Berichte, Forschungszentrum Karlsruhe, Germany, 2000. 11448

Thompson, A. M., Witte, J. C., McPeters, R. D., Oltmans, S. J., Schmidlin, F. J., Logan, J. A., Fujiwara, M., Kirchhoff, V. W. J. H., Posny, F., Coetzee, G. J. R., Hoegger, B., Kawakami, S., Ogawa, T., Johnson, B. J., Vömel, H., and Labow, G.: Southern Hemisphere Additional Ozonesondes (SHADOZ) 1998–2000 tropical ozone climatology 1. Comparison with Total Ozone Mapping Spectrometer (TOMS) and ground-based measurements, J. Geophys. Res., 108, 8238, doi:10.1029/2001JD000967, 2003. 11452

Tikhonov, A.: On the Solution of Incorrectly Stated Problems and a Method of Regularisation, Dokl. Acad. Nauk SSSR, 151, 501–504, 1963. 11447

Tjemkes, S. A., Patterson, T., Rizzi, R., Shephard, M. W., Clough, S. A., Matricardi, M., Haigh, J. D., Höpfner, M., Payan, S., Trotsenko, A., Scott, N., Rayer, P., Taylor, J. P., Clerbaux, C., Strow, L. L., DeSouza-Machado, S., Tobin, D., and Knuteson, R.: The ISSWG line-by-line inter-comparison experiment, J. Quant. Spectrosc. Ra., 77, 433–453, doi:10.1016/S0022-4073(02)00174-7, 2003. 11446

Turquety, S., Hadji-Lazaro, J., and Clerbaux, C.: First satellite ozone distributions re-

trieved from nadir high-resolution infrared spectra, Geophys. Res. Lett., 29, 2198, doi:10.1029/2002GL016431, 2002. 11444

Turquety, S., Hadji-Lazaro, J., Clerbaux, C., Hauglustaine, D. A., Clough, S. A., Cassé, V., Schlüssel, P., and Mégie, G.: Operational trace gas retrieval algorithm for the Infrared Atmospheric Sounding Interferometer, J. Geophys. Res., 109, D21301, doi:10.1029/2004JD004821, 2004. 11447, 11451

von Clarmann, T. and Grabowski, U.: Elimination of hidden a priori information from remotely sensed profile data, Atmos. Chem. Phys., 7, 397–408, 2007, http://www.atmos-chem-phys.net/7/397/2007/. 11457

Worden, H. M., Logan, J. A., Worden, J. R., Beer, R., Bowman, K., Clough, S. A., Eldering, A., Fisher, B. M., Gunson, M. R., Herman, R. L., Kulawik, S. S., Lampel, M. C., Luo, M., Megretskaia, I. A., Osterman, G. B., and Shephard, M. W.: Comparisons of Tropospheric Emission Spectrometer (TES) ozone profiles to ozonesondes: Methods and initial results, J. Geophys. Res., 112, D03309, doi:10.1029/2006JD007258, 2007. 11444

Worden, H. M., Bowman, K. W., Eldering, A., and Beer, R.: Satellite measurements of the clear-sky greenhouse effect from tropospheric ozone, Nature Geoscience, 1, 305–308, doi:10.1038/ngeo182, 2008. 11444

Table 1. summary of all sounding stations used in this study.

Name	archive	latitude	longitude	altitude	sensor[a]	correction factor[c]	applied[b]	used coincidences[d]
midlatitude sondes								
Boulder (Colorado, USA)	GMD	40.0N	105.2W	1743m	ECC	0.98	no	35
Payerne (Switzerland)	NADIR	46.8N	7.0E	491m	ECC	1.01	no	99
STN012 (Sapporo, Japan)	WOUDC	43.1N	141.3E	26m	KC-96	0.99	yes	32
STN014 (Tateno, Japan)	WOUDC	36.1N	140.1E	31m	KC-96	0.96	yes	46
STN107 (Wallops Island, USA)	WOUDC	37.9N	75.5W	13m	ECC	1.00	no	28
STN174[e] (Lindenberg, Germany)	WOUDC	52.2N	14.1W	112m	ECC	0.98	yes	57
STN221 (Legionowo, Poland)	WOUDC[f]	52.4N	21.0E	96m	ECC	0.98	no	48
STN308[e] (Barajas, Spain)	WOUDC	40.5N	3.6W	631m	ECC	0.98	no	46
STN318[e] (Valentia Obs., Ireland)	WOUDC	51.9N	10.2W	14m	ECC	0.93	no	58
midlatitude sondes (not processed by LATMOS)								
De Bilt (The Netherlands)	NADIR	52.1N	5.2E	4m	ECC	1.02	no	43
Hohenpeißenberg (Germany)	NADIR	47.8N	11.0E	976m	BM	1.07	yes	72
Lerwick (Shetland, Great Britain)	NADIR	60.1N	1.2W	82m	ECC	1.00	no	71
Sodankylä (Finland)	NADIR	67.4N	26.6E	179m	ECC	1.00	no	79
Uccle (Belgium)	NADIR	50.8N	4.4E	100m	ECC	0.97	yes	107

[a] ECC: electrochemical cell, KC: modified Japanese ECC (see text), BM: Brewer-Mast
[b] indicates, whether the correction factor was applied to the measured ozone profiles
[c] the ratio between ozone total columns measured by a UV-spectrometer and by the ozone sonde, averaged over all used coincidences
[d] number of all cloud-free coincidences between IASI and sondes which are used in the comparison
[e] these three sondes are processed by LPMAA
[f] from 1.5.08 on, the sonde data was taken from NADIR

ACPD
9, 11441–11479, 2009

Table 2. Summary of the statistics of the distribution of the differences between ozone partial columns retrieved from IASI and from sonde measurements. For the different teams, we present the average (μ) and the standard deviation (σ) for both, the comparison of IASI with the raw sonde profiles and with the sonde profile convolved with the averaging kernels. A graphical presentation of the statistics is shown in Fig. 5

			with raw sonde						with convolved sonde					
team	time period		0–6 km		0–11 km		0–14 km		0–6 km		0–11 km		0–14 km	
sonde selection			μ[a]	σ[a]	μ	σ	μ	σ	μ	σ	μ	σ	μ	σ
LISA	6.07–8.08	[DU]	1.4	4.7	−0.3	7.8	−2.1	9.5	1.0	3.4	0.5	6.7	−2.1	9.4
all mid-latitude sondes		[%]	5.5	24.1	−0.9	22.0	−4.1	16.3	4.8	18.0	1.1	17.8	−4.1	15.7
LATMOS	6.07–8.08	[DU]	3.5	4.2	0.3	6.0	−2.6	8.0	0.3	1.1	−1.7	3.5	−3.9	6.4
selected mid-lat. sondes[b]		[%]	13.5	17.7	0.8	17.6	−6.7	15.6	1.3	6.1	−5.6	10.5	−8.4	11.6
EUMETSAT	2.08–8.08	[DU]	−5.5	5.7	−5.3	6.9	−3.5	9.5	–	–	–	–	–	–
all mid-latitude sondes		[%]	−26.3	27.1	−14.0	18.1	−7.5	17.1	–	–	–	–	–	–
LISA	2.08–8.08	[DU]	0.5	4.8	−2.8	6.9	−2.8	8.7	−0.2	3.4	−2.1	6.0	−5.1	8.0
all mid-latitude sondes		[%]	2.3	22.4	−7.7	18.9	−4.9	14.8	−2.3	16.5	−6.0	15.8	−8.4	13.8

[a] the distribution of (sonde-IASI) is assumed to be Gaussian with μ: mean and σ: standard deviation;
[b] e.g. the upper part in Table 1.

ACPD
9, 11441–11479, 2009

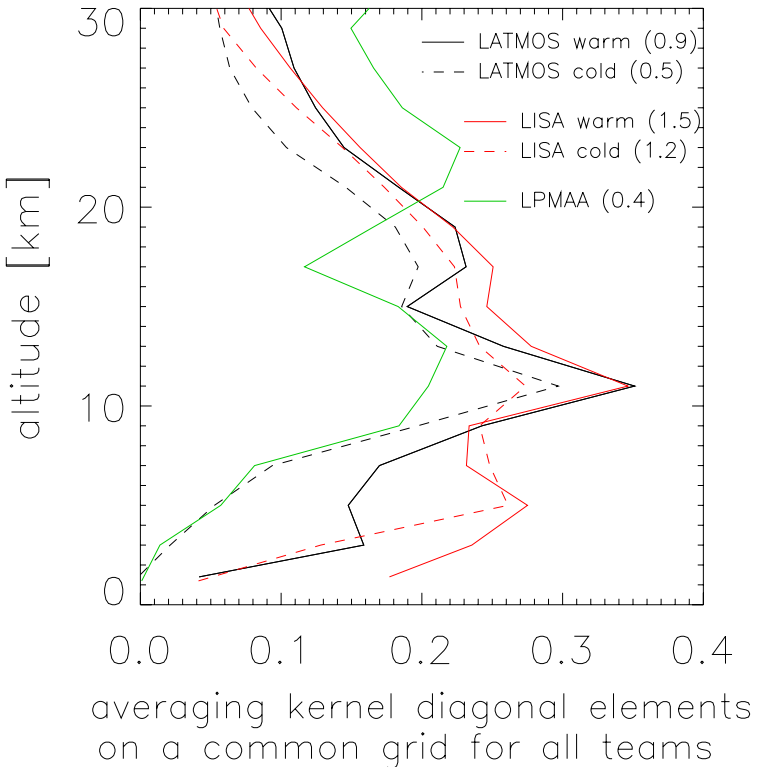

Fig. 1. Comparison of the diagonals of the averaging kernel matrix of different profile retrieval approaches on a common grid (see Eq. 6). As examples we chose a cold case (surface temperature about 278 K) and a warm case (302 K) around the station in Barajas, Spain. For the retrieval at LPMAA, only mean averaging kernels are available. In parentheses we give the DOF for the column from the surface up to 11 km.

ACPD
9, 11441–11479, 2009

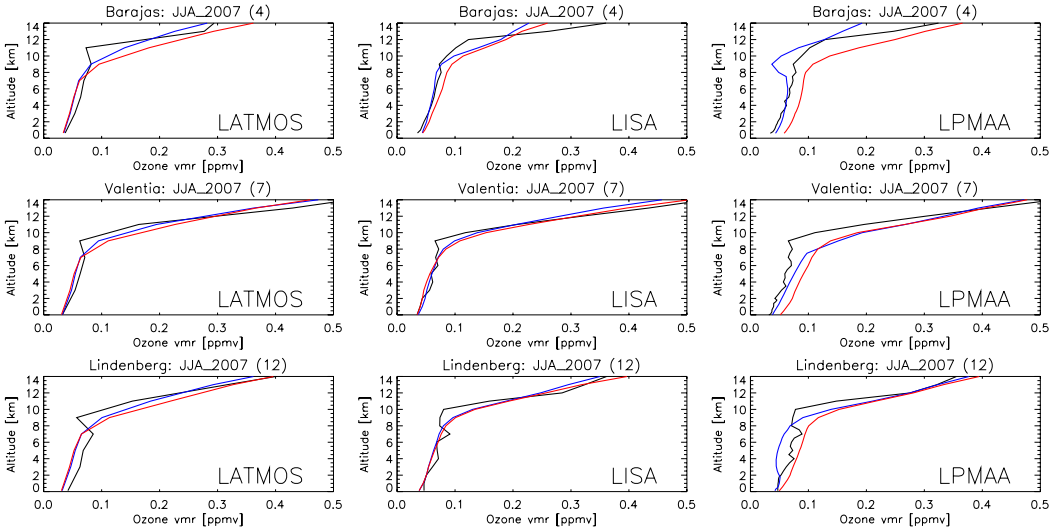

Fig. 2a. Comparison between averages of retrieved IASI-profiles (red), interpolated sonde (black), and AK-smoothed sonde (blue) for three European stations (Barajas(Spain), Valentia(Ireland), and Lindenberg(Germany)). The averaging period is summer (JJA) 2008. The left column shows retrievals performed at LATMOS, the middle column shows retrievals performed at LISA, and the right shows retrievals performed at LPMAA. In parentheses we give the number of used coincidences in the average.

ACPD
9, 11441–11479, 2009

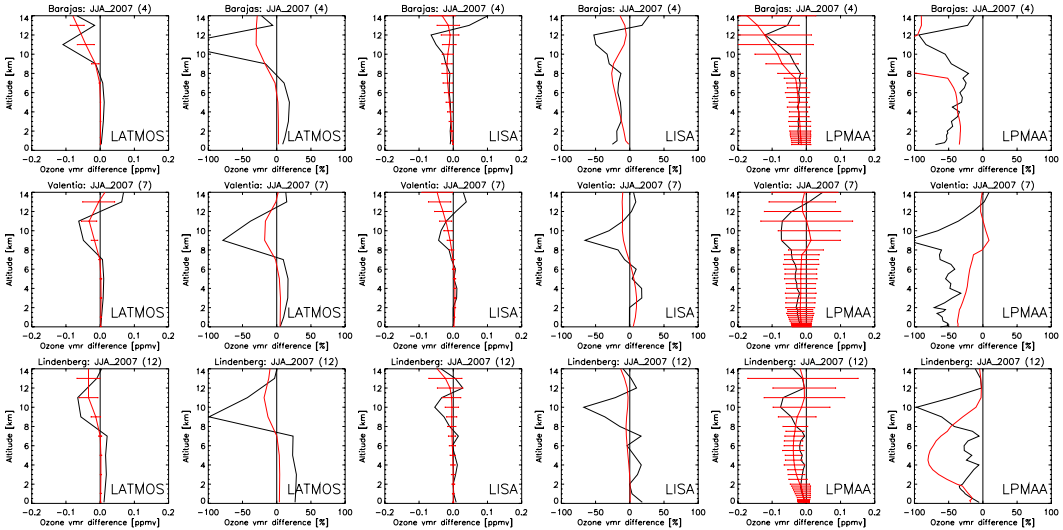

Fig. 2b. Same as Fig. 2a, but with the differences (sonde – retrieval, black) and (AK-smoothed sonde – retrieval, red). The relative differences are calculated with respect to the sonde profiles. The bars give the variability (1σ) of the difference, not the errors associated with the profiles.

ACPD
9, 11441–11479, 2009

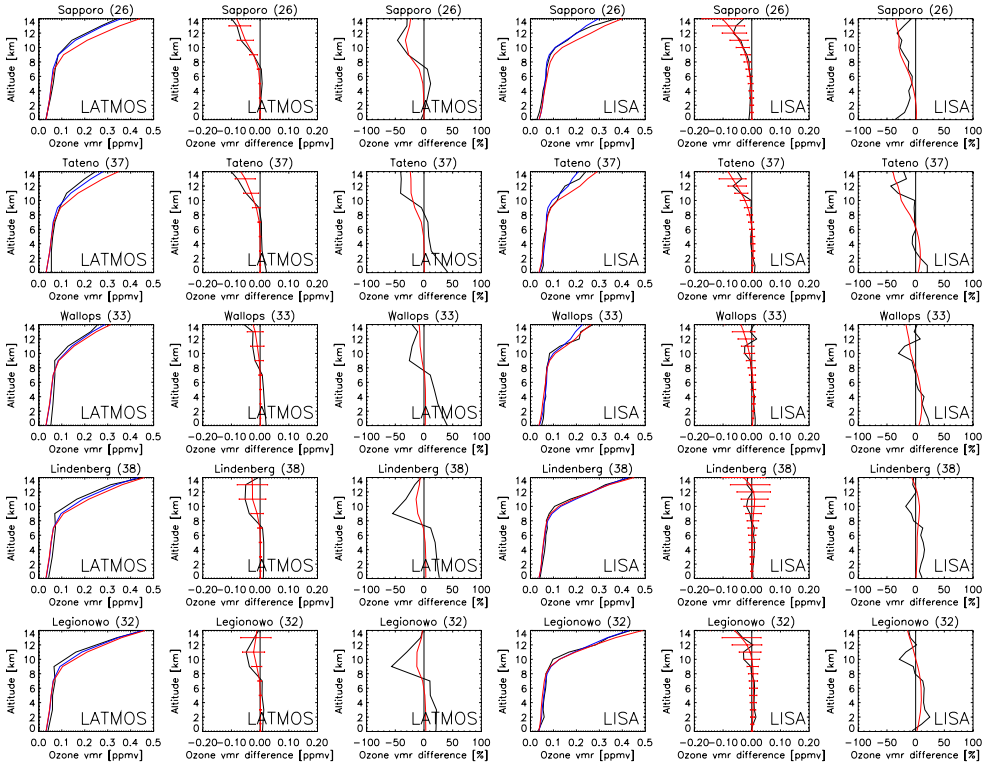

Fig. 3a. Comparison between averages of retrieved IASI-profiles (red), interpolated sonde (black), and AK-smoothed sonde (blue) for all mid-latitude stations processed by LATMOS and LISA. The averaging period is June 2007–August 2008. The left columns shows profiles and the differences for retrievals performed at LATMOS, the right columns show the same for LISA. The relative differences are calculated with respect to the sonde profiles. In parentheses we give the number of used coincidences in the average, the bars give the variability (1σ) of the difference.

ACPD
9, 11441–11479, 2009

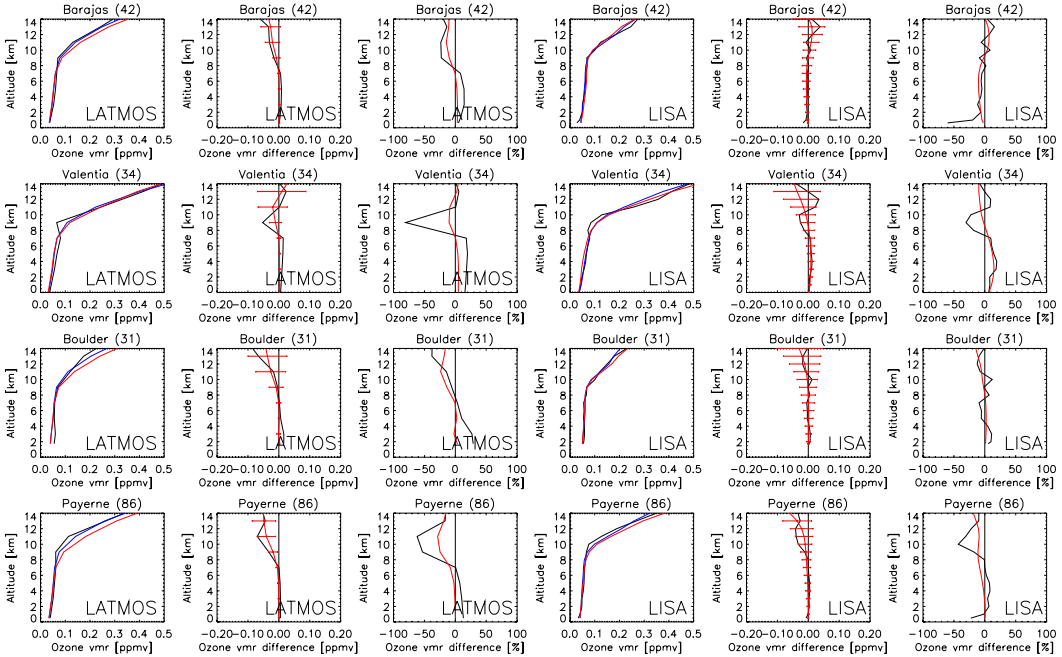

Fig. 3b. Same as Fig. 3a, but with other locations.

ACPD
9, 11441–11479, 2009

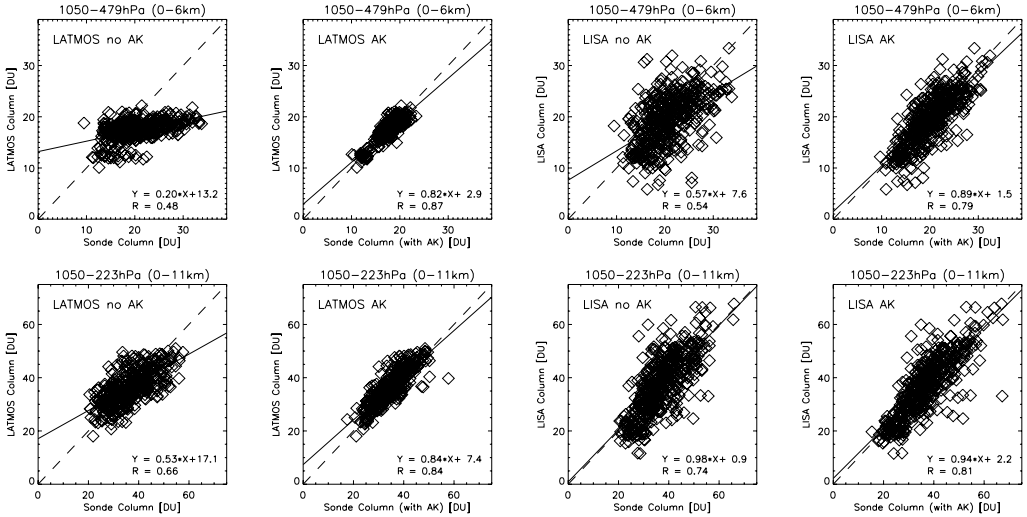

Fig. 4. Comparison of the IASI-retrievals performed at LISA and LATMOS for mid-latitude stations for the period June 2007–August 2008.

ACPD
9, 11441–11479, 2009

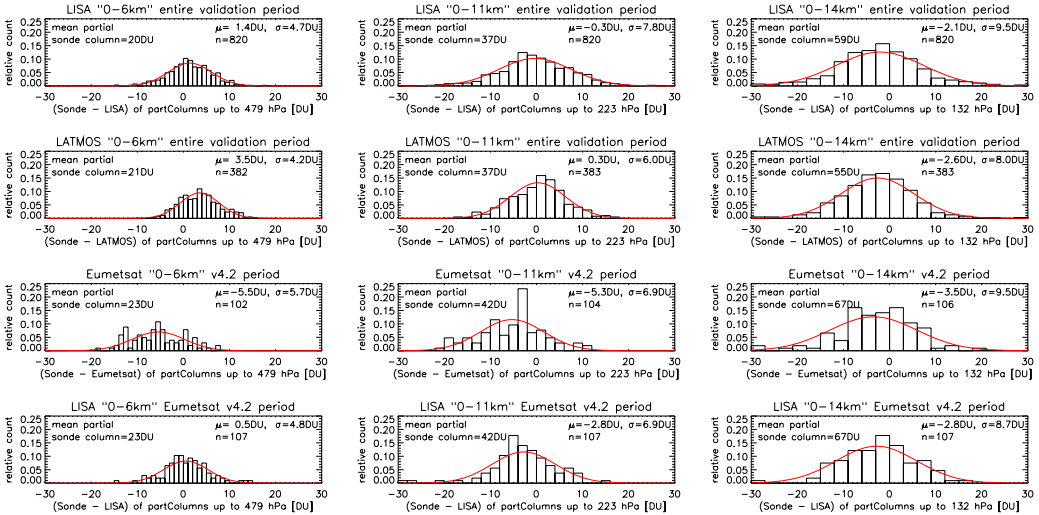

Fig. 5. Bias(μ) and variability(σ) of the differences between the IASI- retrievals (LATMOS, LISA, and EUMETSAT) and the ozone sondes, calculated from n coincidences for the three partial columns: about 0–6 km, 0–11 km, and 0–14 km. We show only the absolute differences with the raw sonde measurements, for the results with the AK-smoothed sonde profiles and the relative differences, we refer to the text and to Table 2.

ACPD
9, 11441–11479, 2009

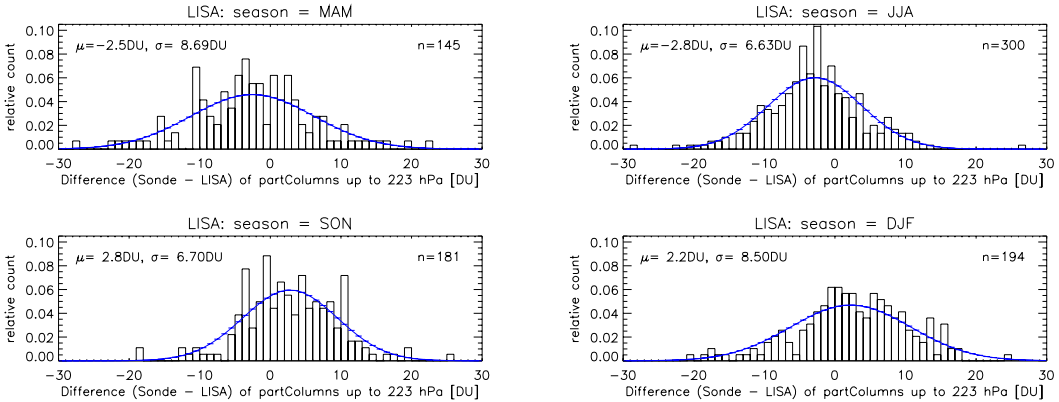

Fig. 6. Bias(μ) and variability(σ) of the differences between the columns from the surface up to 223 hPa from the LISA-retrievals and the sonde measurements for the four seasons, calculated from n coincidences.

ACPD
9, 11441–11479, 2009

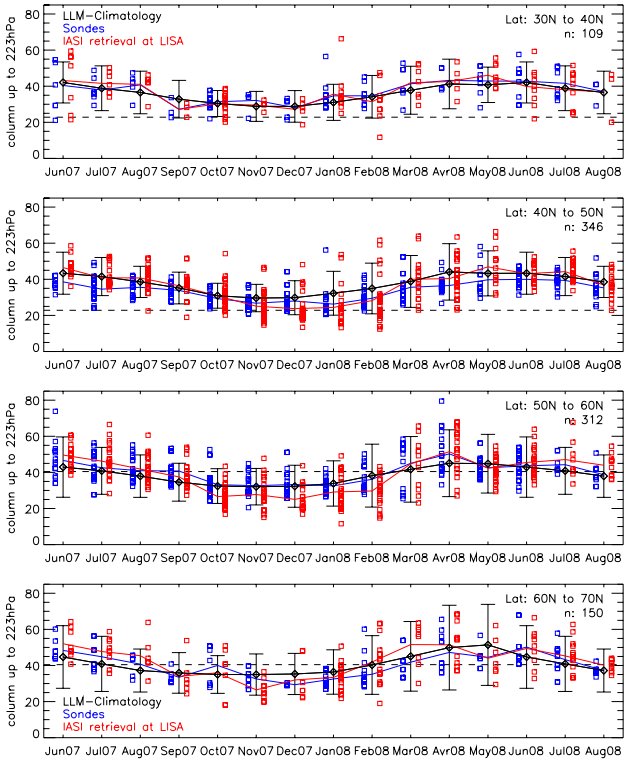

Fig. 7. Annual variability of the ozone column from the surface up to 223 hPa for different northern latitude bands. We show the individual measurements (symbols) together with the means (lines). We give the sonde measurements (blue), the IASI-retrieval performed at LISA (red), and the Labow, Logan, McPeters (LLM) climatology (McPeters et al., 2007, black). The bars indicate the variability (3σ) given in the climatology. The dashed line indicates the column of the a priori profile. The number of used coincidences is n.

ACPD
9, 11441–11479, 2009